Simulation Study of Al-1Mn/Al-10Si Circular Clad Ingots Prepared by Direct Chill Casting

LI WU, HUIJUN KANG, ZONGNING CHEN, YING FU, and TONGMIN WANG

A modified direct chill casting process based on Novelis Fusion™ Technology co-casting process was used recently to prepare Al-1Mn/Al-10Si circular clad ingots. In the current study, a comprehensive simulation model was developed to investigate the direct chill casting process for preparing the Al-1Mn/Al-10Si circular clad ingots, and a parametric study and experimental research of the direct chill casting process was conducted to explore potential success and failure casting conditions. The simulation results revealed the bonding mechanism of the Al-1Mn/Al-10Si interface in the direct chill casting process and identified the effect of certain parameters on casting performance. The results indicated that the effect of casting speed and Al-1Mn casting temperature on the variations of the minimum solid fraction of Al-1Mn at the interface is stronger than that of cooling water flow rate in inner mold, while Al-10Si casting temperature is the weakest of the four casting parameters. The corresponding experimental results verified that Al-1Mn/Al-10Si circular clad ingot with acceptable metallurgical bonding can be successfully prepared by direct chill casting process under the proper casting parameters. The thickness of diffusion zone is about 40 μm, and the fractured position in tensile test was located in the Al-1Mn alloy side which indicated the strength of the interfacial region is higher than that of Al-1Mn alloy.

DOI: 10.1007/s11663-015-0473-0

I. INTRODUCTION

ALUMINUM clad products have been successfully used in the automotive industry and others, since they exhibit an excellent combination of physical, chemical, and mechanical properties that cannot be achieved by a monolithic material.[1] The automotive heat exchanger is an important application of the aluminum clad product which is made from a corrosion-resistant alloy at internal layer with a thin clad layer of a brazing alloy. The main conventional method for cladding products is roll bonding,[2,3] which has served the industry well for decades. However, a major disadvantage is that roll bonding is a very time intensive and expensive process, and it is impossible to remove all of the oxides at the interface.[4]

For the past few years, the process of simultaneous casting was developed for the manufacturing of clad products. This casting process has the distinct advantages of both cost reduction and interface improvement. For example, a new Novelis Fusion™ Technology for the manufacturing of clad aluminum products was introduced in some literature.[5,6] The copper cladding aluminum rods were fabricated by Su *et al.* using horizontal core-filling continuous casting technology.[7] The clad aluminum hollow billets were prepared by Liu *et al.* using horizontal continuous casting.[8] An 8090/3003 bimetal slab with consistent mechanical properties was prepared by Wang *et al.* using a modified direct chill casting process.[9] A continuous composite casting process was developed by Nerl *et al.* for the production of bilayer aluminum strips.[10] In order to understand the casting process, several models were developed to analyze the casting process by many researchers with the development of powerful numerical methods and computers.[11–16] For instance, Yoon[12] reviewed the applications of numerical simulations to continuous casting technology in steel production. Foroozmehr *et al.*[15] described a coupled dissolution and diffusion model of solutionizing and solute redistribution in a co-cast bilayer aluminum alloy system. Baserinia *et al.*[14] developed a steady-state thermofluids model of the Fusion™ Technology co-casting process to simulate the casting of rectangular bimetallic ingots. Caron *et al.*[16] used the three-dimensional numerical thermofluids model to simulate the co-casting of AA3003/AA4045 clad rectangular ingots *via* Fusion™ Technology with an asymmetrical arrangement of feeding systems.

In our previous research, a modified direct chill casting process based on Novelis Fusion™ Technology co-casting process was used to prepare Al-1Mn/Al-10Si circular clad ingots.[17] As is known, the Al-1 wt pctMn alloy has excellent corrosion resistance and low strength, while the Al-10 wt pctSi alloy (all in wt pct if not stated otherwise) has high strength, weldability, and poor

LI WU, Ph.D. Student, YING FU, Postdoctoral Fellow, and TONGMIN WANG, Professor, are with the Key Laboratory of Solidification Control and Digital Preparation Technology (Liaoning Province), School of Materials Science and Engineering, Dalian University of Technology, No. 2 Linggong Road, Ganjingzi District, Dalian City, Liaoning Province 116024, P. R. China. Contact e-mail: tmwang@dlut.edu.cn HUIJUN KANG, Lecturer, and ZONGNING CHEN, Postdoctoral Fellow, are with the Laboratory of Special Processing of Raw Materials, Dalian University of Technology, Dalian 116024, P. R. China.

Manuscript submitted January 23, 2015.
Article published online October 13, 2015.

corrosion resistance. Therefore, the Al-1Mn and Al-10Si circular clad ingot prepared by the direct chill casting process can combine their advantages. In the current study, a comprehensive simulation model was developed to investigate the direct chill casting process for preparing the Al-1Mn/Al-10Si circular clad ingot, and a parametric study and experimental research of the direct chill casting process was conducted to explore the potential success and failure casting conditions.

II. EXPERIMENTS

Figure 1 presents the schematic of the vertical direct chill casting process for preparing the circular clad ingot. 1. Al-1Mn and Al-10Si alloys are selected as the clad layer and core layer materials, respectively. The Al-1Mn pouring tundish is fixed on the top of the outer mold. The water-cooled stainless steel sleeve (inner mold) with heat insulator on its inner and bottom side is placed in the center of the outer mold. The diameter of clad ingot is 160 mm, and the core Al-10Si alloy has a diameter of 80 mm. As presented in Figure 1, molten metal of the clad layer is poured into the outer mold and contact with the inner mold firstly. A primary semisolid shell of Al-1Mn alloy is formed after contacting with the lower part of inner mold and pulled down as the starter block is withdrawn at a given casting speed. The core layer melt is then poured into the inner mold and makes first contact with the semisolid shell immediately below the inner mold. Once the starter block exits the bottom of the outer mold, the clad ingot is cooled directly by the cooling water. This process continues until a clad ingot with a desired height is produced.

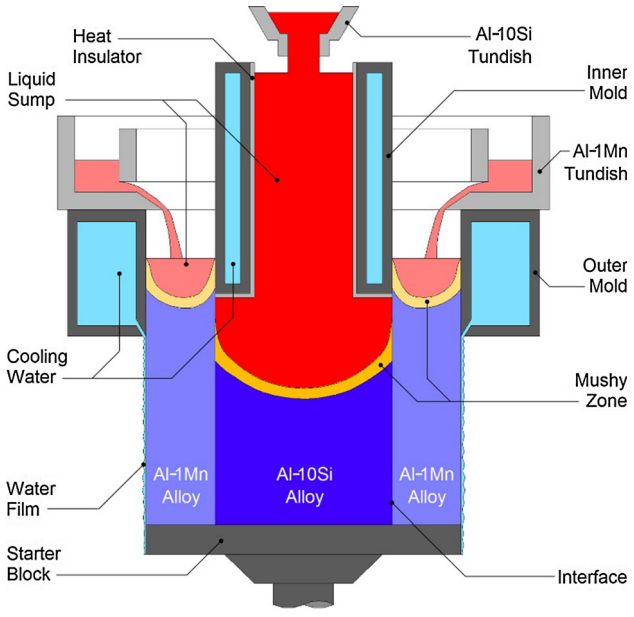

Fig. 1—Schematic of the vertical direct chill casting process for preparing the circular clad ingot.

III. SIMULATION MODEL

A. *Assumptions*

To simplify the problem, certain assumptions were made:

(1) The molten aluminum alloys behave as an incompressible fluid.
(2) Ignore the effect of liquid surface fluctuations in the flow.
(3) The calculation of the solute field is not included in this model.
(4) Ignore the interface reaction between Al-1Mn and Al-10Si alloys.

B. *Governing Equations*

Continuity equation:

$$\frac{\partial \rho}{\partial t} + \nabla \cdot (\rho \vec{v}) = 0 \qquad [1]$$

Momentum equation:

$$\frac{\partial (\rho \vec{v})}{\partial t} + \nabla \cdot (\rho \vec{v} \vec{v}) = \nabla \cdot (\mu_{\text{eff}} \nabla \vec{v}) - \nabla P - \frac{\mu_l f_S^2}{K_0 (1 - f_S)^3 + \delta} (\vec{v} - \vec{v}_s) - \rho \vec{g} \beta (T - T_0) \qquad [2]$$

Here, $\vec{v}$ is the fluid velocity; ρ is the density; μ_{eff} is the effective viscosity coefficient, where $\mu_{\text{eff}} = \mu_l + \mu_t$, μ_l is the laminar viscosity and μ_t is the turbulent viscosity; P is the pressure; f_S is the solid volume fraction, respectively; T is the temperature; T_0 is the reference temperature and is assumed to be equal to the liquidus temperature in the current study; δ is a small number to prevent division by zero; K_0 is the permeability factor of the mushy metal; $\vec{v}_s$ is the solid velocity due to the pulling of solidified material out of the domain; g is the gravitational acceleration; and β is the thermal expansion coefficient of the molten aluminum.

The last term in Eq. [2] is the Boussinesq approximation for the thermal buoyancy term. The second last term on the right-hand side of Eq. [2] is Darcy source term. When $0 < f_S \le 0.3$[18], the solid convection is considered and the Darcy flow is not important. Then, the value of the Darcy source term is applied to zero and the laminar viscosity is set as $\mu_l \times 10^{10 f_S}$[19] in Eq. [2].

In this model, the Scheil-type nonequilibrium relationship is used to calculate the solid fraction f_s and the liquid fraction f_L, which are functions of temperature and are expressed using the following equations:

$$f_s = \begin{cases} 0 & T \ge T_L \\ 1 - \left(\frac{T_f - T}{T_f - T_L}\right)^{\frac{1}{k_p - 1}} & T_s < T < T_L \\ 1 & T \le T_s \end{cases} \quad \text{and} \quad f_L = 1 - f_s \qquad [3]$$

Here, k_p is the equilibrium distribution coefficient, T_f is the fusion temperature of the pure base metal, and T_L

and T_S are the liquidus and solidus temperatures, respectively.

The standard k–ε model, which is a semi-empirical model, is used to model the transport of turbulence kinetic energy k and its dissipation rate ε. The first form of this model is

$$\mu_t = \rho C_\mu \frac{k^2}{\varepsilon}, \quad [4]$$

where C_μ is a function of the turbulent Reynolds number, which is a constant value; k and ε represent the turbulence kinetic energy and its rate of dissipation, respectively, and are obtained using the following transport equations:

$$\frac{\partial(\rho k)}{\partial t} + \nabla \cdot (\rho \vec{v} k) = \nabla \cdot [(\mu + \frac{\mu_t}{\sigma_k})\nabla k] + G - \rho\varepsilon \quad [5]$$

$$\frac{\partial(\rho \varepsilon)}{\partial t} + \nabla \cdot (\rho \vec{v} \varepsilon) = \nabla \cdot [(\mu + \frac{\mu_t}{\sigma_\varepsilon})\nabla \varepsilon] + c_1 \frac{\varepsilon}{k} G - c_2 \rho \frac{\varepsilon^2}{k}, \quad [6]$$

where $G = -\rho \overline{v'_i v'_j}(\partial v_j / \partial x_i)$, $c_1 = 1.44$, $c_2 = 1.92$, $c_\mu = 0.09$, $\sigma_k = 1.0$, and $\sigma_\varepsilon = 1.3$.

Energy equation:

$$\frac{\partial(\rho H)}{\partial t} + \nabla \cdot (\rho \vec{v} H) = \nabla \cdot (k \nabla T) \quad [7]$$

The enthalpy of the material H is computed as the sum of the sensible enthalpy $h = \int_{T_{ref}}^{T} c_p dT$ and the latent heat $\Delta H = f_L \Delta H_f$ in the energy equation as

$$H = \int_{T_{ref}}^{T} c_p dT + f_L \Delta H_f, \quad [8]$$

where $\vec{v}$ is the fluid velocity, k is the thermal conductivity, T_{ref} is the reference temperature, C_p is the specific heat at constant pressure, f_L is the liquid fraction, and ΔH_f is the latent heat of the material.

C. *Material Properties and Boundary Conditions*

Al-1Mn and Al-10Si alloys are used as the experiment materials of the internal and external layers of the circular clad ingot, respectively, in the current study. Al-1Mn alloy is a high melting-point corrosion-resistant alloy and Al-10Si alloy is a lower melting-point brazing alloy. Table I lists the material properties of Al-1Mn and Al-10Si used in this simulation. The material properties of Al-1Mn and Al-10Si are based on that of AA3003 and AA4045, respectively, used by Baserinia *et al.*[14] for nonequilibrium solidification. Here, the solid fraction changing with the temperature presented in Figure 2(c) is based on the Scheil type nonequilibrium relationship, and the eutectic solidification of Al-10Si is assumed to occur from 861 K to 851 K (588 °C to 578 °C) in order to avoid numerical instabilities.

In order to model the casting processes, the governing equations of the flow field and thermal field were solved using the commercial software ANSYS-FLUENT. Figure 3 shows the geometry model, computational grid, and boundary conditions. The outer mold and inner mold are 65 and 120 mm in height, respectively. The height level difference between the bottom of the inner mold and outer mold is 25 mm. The Al-1Mn melt surface is 45 mm higher than the bottom of the outer mold. The size of the circular clad ingot is Φ160 mm with a simulation height of 420 mm and the thickness of the external layer Al-1Mn alloy is 35 mm. For the axisymmetric distribution of the circular clad ingot, an axisymmetric model was used to reduce the calculation amount, as shown in Figures 3(b) and (c).

As illustrated in Figure 3(c), when the flow field and thermal field of the casting process are solved, the boundary conditions are described as follows.

1. *Inlet and outlet boundary*

The velocity boundary condition is used in the region. The turbulence kinetic energy and its dissipation rate are set as follows:

$$k_{inlet} = 0.01 u_{inlet}^2;\ \varepsilon_{inlet} = \frac{k_{inlet}^{1.5}}{R_{inlet}};\ k_{outlet} = 0;\ \varepsilon_{outlet} = 0 \quad [9]$$

Table I. Material Properties

Property	Al-1Mn	Al-10Si
Density (kg m^{-3})	2400	2408
Viscosity (kg m^{-1} s^{-1})[14]	0.00115	0.00115
Specific heat (J kg^{-1} K^{-1})[14]	as shown in Figure 2(a)	as shown in Figure 2(a)
Thermal conductivity (W m^{-1} K^{-1})[14]	as shown in Figure 2(b)	as shown in Figure 2(b)
Thermal expansion coefficient (K^{-1})[14]	2.3×10^{-5}	2.1×10^{-5}
Permeability factor (m^2)[14]	6.67×10^{-11}	6.67×10^{-11}
Latent heat of fusion (J kg^{-1})[14]	4.08×10^5	4.60×10^5
Solidus temperature [K(°C)][14]	858 (585)	851 (578)
Coherency temperature [K(°C)][14]	922 (649)	858 (585)
Liquidus temperature [K(°C)][14]	927 (654)	871 (598)
Equilibrium distribution coefficient	0.67	0.13
Solid fraction[14]	as shown in Figure 2(c)	as shown in Figure 2(c)

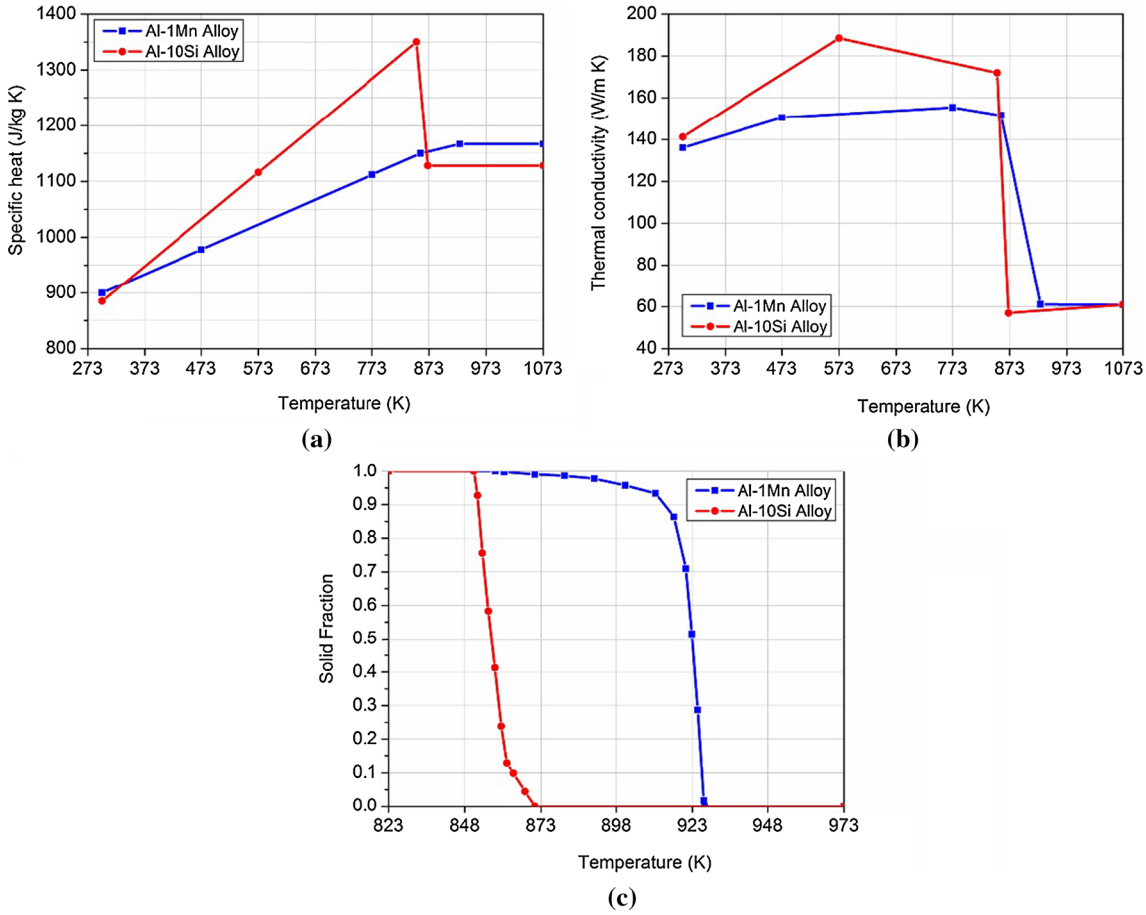

Fig. 2—(*a*) Specific heat, (*b*) thermal conductivity, and (*c*) solid fraction of Al-1Mn and Al-10Si.

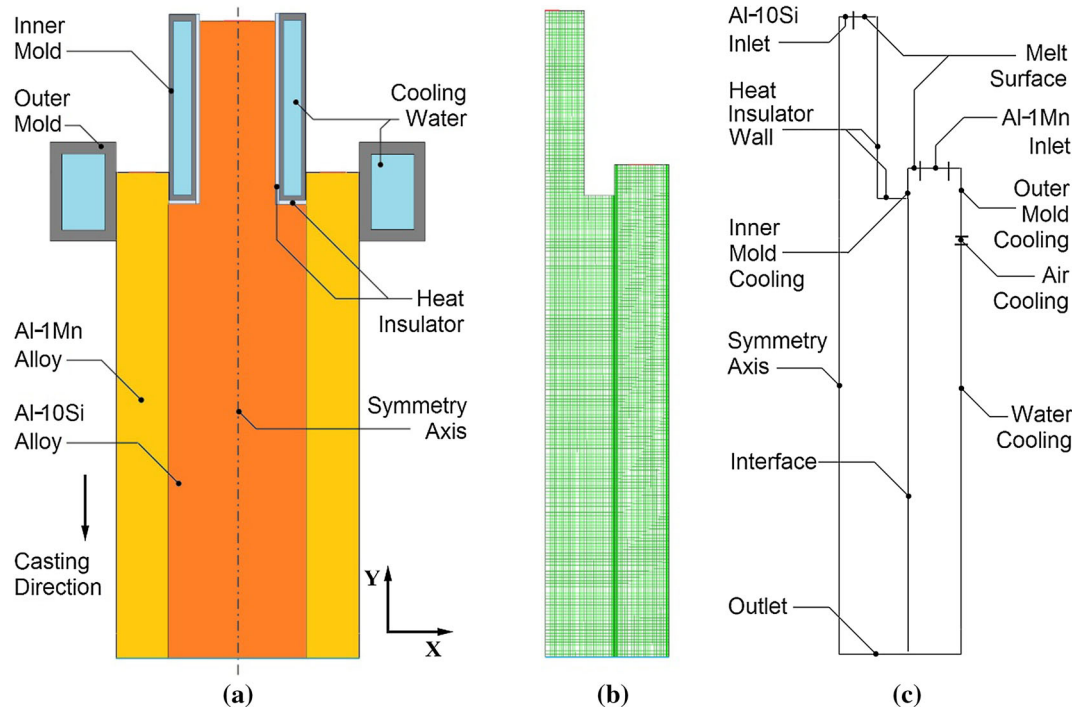

Fig. 3—Geometry model (*a*), computational grid (*b*), and boundary conditions (*c*) in ANSYS-FLUENT.

where R_{inlet} is the hydraulic radius of the inlet. The temperatures at the inlet and outlet boundaries are set to the pouring temperature and room temperature, respectively.

2. *Mold cooling boundary*

The thermal boundary condition is treated as Cauchy-type boundary condition, and the heat transfer coefficient between the mold and the metal is assumed to vary with the solid fraction and is written according to Eq. [10]:[20]

$$h_{mold} = h_{contact} \times (1 - f_S) + h_{gap} \times f_S, \quad [10]$$

where $h_{contact}$ is intended to reflect good thermal contact with the mold and is in the range of 1000 to 2000 W m^{-2} K^{-1} due to the different cooling water flow rate in the mold, h_{gap} is given as 100 W m^{-2} K^{-1} to reflect poor thermal contact associated with the gap formed when the metal is solidified.

3. *Water cooling boundary*

The water cooling boundary condition used in the current model is based on the empirical model of Weckman and Niessen.[21] The forced convection and nucleate boiling effects are estimated for a turbulent water film of water on a vertical surface. For forced convection, the heat transfer coefficient is given as follows[16,21]:

$$h_{conv} = [-1.67 \times 10^5 + 352(T_{surf} + T_w)]Q'^{1/3}, \quad [11]$$

where T_{surf} and T_w are the clad ingot surface temperature and the local cooling water temperature in Kelvin, and Q' is the volume flow rate of cooling water per unit circumference in m^2 s^{-1} and its specific value is about 6.63×10^{-4} m^2 s^{-1} in the current study. When nucleate boiling takes place, the heat transfer coefficient is given as follows:[16,21]

$$h_{NB} = [-1.67 \times 10^5 + 352(T_{surf} + T_w)]Q'^{1/3} + 20.8(T_{surf} - T_{sat})^3, \quad [12]$$

where T_{sat} is the water saturation temperature equal to 373 K (100 °C). Therefore, the heat transfer coefficient in water cooling zone is determined according to the following equations:

$$h_{water} = \begin{cases} h_{conv} & \text{for } h_{conv}(T_{surf} - T_w) < 3910(T_{surf} - T_{sat})^{2.16} \\ h_{NB} & \text{for } h_{conv}(T_{surf} - T_w) \geq 3910(T_{surf} - T_{sat})^{2.16} \end{cases}, \quad [13]$$

where the local cooling water temperature $T_w(y)$ is calculated by integrating the heat absorbed via water cooling zone at locations above position y:[16]

$$T_w(y) = T_w(0) + \int_0^y \frac{h_{water}(T_{surf} - T_w)}{Q'\rho_w C_{p,w}} dy, \quad [14]$$

where ρ_w and $C_{p,w}$ are the density (958.6 kg m^{-3}) and specific heat (4251 J kg^{-1} K) of water, respectively.

4. *Air cooling boundary*

The velocity and turbulence boundary conditions are treated as the moving wall, and its moving velocity is the casting speed. The heat transfer coefficient in the air cooling zone is given as follows:

$$h_{air} = \sigma \cdot \varepsilon \cdot T_{surf}^3, \quad [15]$$

where σ is the Stefan–Boltzmann constant (5.67×10^{-8} W m^{-2} K^{-4}) and ε is the Blackness (0.19) of the clad ingot surface.

The heat insulator wall boundary condition is treated as Cauchy-type boundary condition, and the heat transfer coefficient between the heat insulator and the metal is set as 20 W m^{-2} K^{-1} to reflect some heat transfer occurring. The Al-1Mn/Al-10Si interface is modeled as a zero-thickness layer with a discontinuous change in material properties. Momentum and energy are conserved across the interface; however, no mass transfer is allowed. The boundary conditions of the rest of the walls are treated as those of a static adiabatic wall.

IV. RESULTS AND DISCUSSION

In this section, the numerical results of the casting process for preparing Al-1Mn/Al-10Si circular clad ingots based on the simulation model explained before are presented and discussed. First, the results are presented for a typical case to understand the physics of the casting process, and then, a parametric study is performed to identify the effect of certain parameters on casting performance. Finally, corresponding experimental results are shown to verify the simulation work.

A. *Physics of the Casting Process*

As the first typical test case, the casting speed (v_{cast}) is 60 mm min^{-1}, the casting temperature of Al-1Mn melt ($T_{cast\_Al\text{-}1Mn}$) and Al-10Si melt ($T_{cast\_Al\text{-}10Si}$) is 993 K and 903 K (720 °C and 630 °C), respectively, and the cooling water flow rate in inner mold (Q_{inner}) and outer mold (Q_{outer}) is 700 and 1200 L h^{-1}, respectively. Figure 4 shows the predicted velocity vectors, velocity contours, temperature contours, and liquid fraction contours during the casting process in the typical case. As seen from Figures 4(a) and (b), the clad layer Al-1Mn and core layer Al-10Si melt are poured into the liquid sump from different inlets and then flow vertically downwards to reach the solidification front with the slight recirculating flow pattern. The maximum velocities of Al-1Mn and Al-10Si melt are 0.0017 and 0.02 m/s at their inlets, respectively. As seen from Figures 4(c) and (d), the clad layer Al-1Mn melt is cooled by the mold and cooling water; however, the heat of core layer Al-10Si melt is only extracted by the clad layer alloy. The temperature contours across the interface are continuous but the liquid fraction contours are discontinuous, this is because the variation of liquid fraction with respect to temperature is different for the Al-1Mn and Al-10Si alloys. The mushy region of

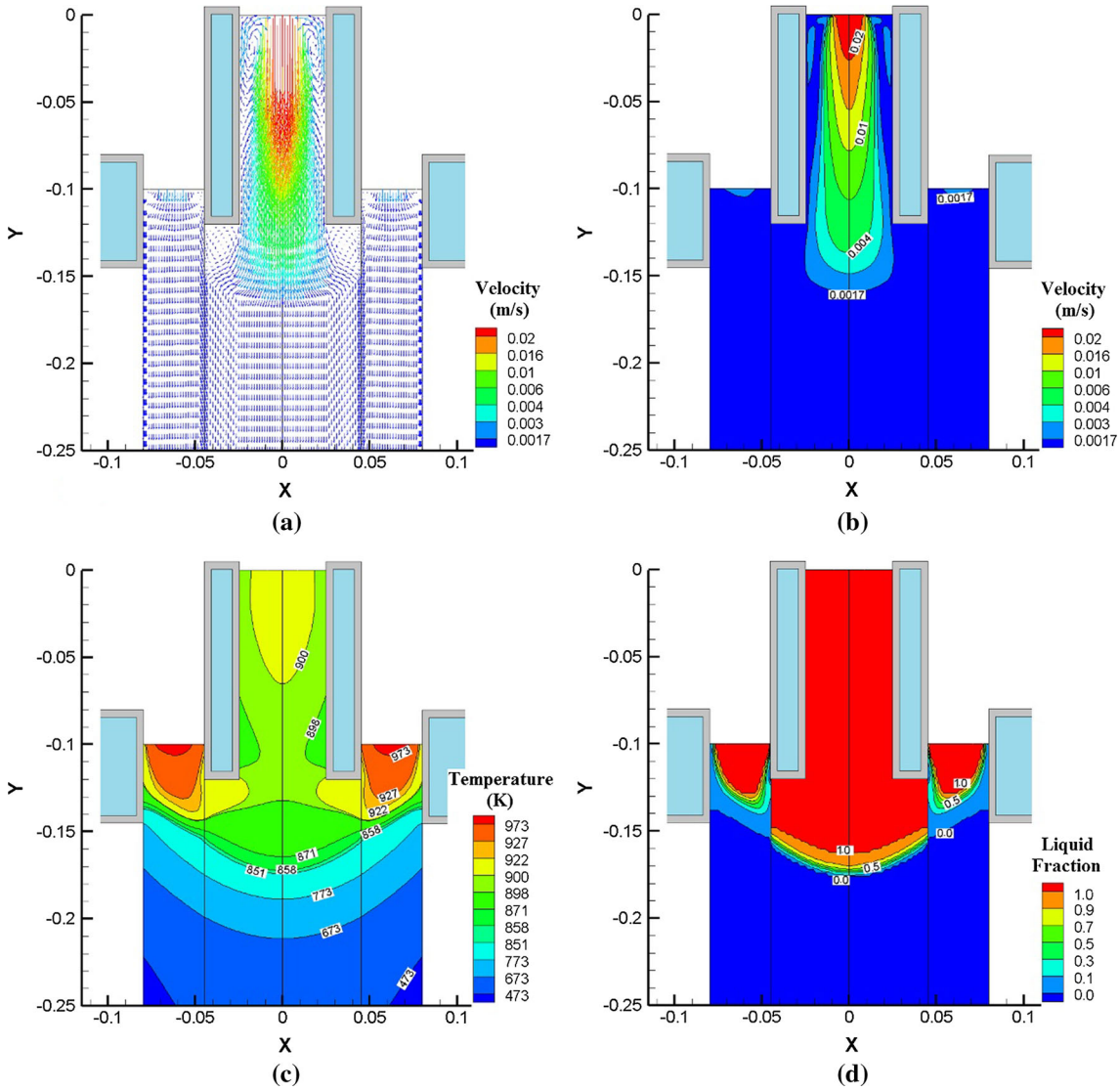

Fig. 4—Calculated results of the typical case: (*a*) velocity vectors, (*b*) velocity contours, (*c*) temperature contours, and (*d*) liquid fraction contours of the clad ingot. (v_{cast} = 60 mm min^{-1}, $T_{cast\_Al\text{-}1Mn}$ = 993 K (720 °C), $T_{cast\_Al\text{-}10Si}$ = 903 K (630 °C), Q_{inner} = 700 L h^{-1}, and Q_{outer} = 1200 L h^{-1}).

Al-1Mn alloy is wider than that of Al-10Si alloy because of the larger difference between liquidus and solidus temperature. The inner mold creates an initial primary shell in the Al-1Mn alloy which grows slowly until it leaves the inner mold and comes in contact with the liquid Al-10Si alloy. At this point, there is some reheating and remelting of the shell due to the hot liquid Al-10Si alloy until it reaches the bottom of the Al-1Mn sump.

Figure 5 shows a plot of the calculated solid fraction of the Al-1Mn and Al-10Si alloys as a function of vertical position at the interface of core and clad layers. As seen, the solid fraction on the Al-1Mn side of the ingot increases initially to 0.95 because of the inner mold cooling. However, this solid fraction reduces to a minimum of 0.88 at the interface zone once it comes into contact with the Al-10Si molten alloy and is reheated. Below this point, the values of solid fraction

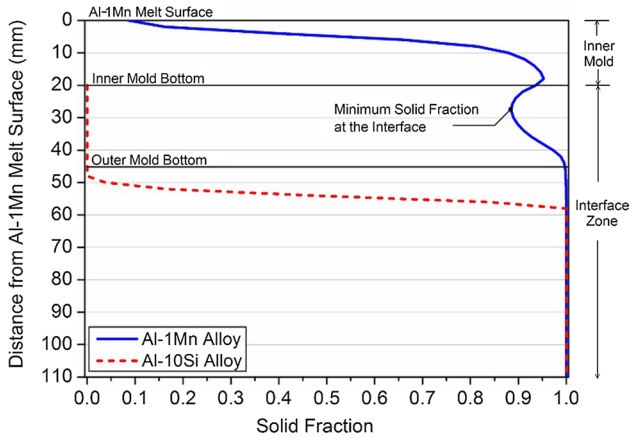

Fig. 5—Calculated variations of solid fraction at the interface of the clad ingot. (v_{cast} = 60 mm min^{-1}, $T_{cast\_Al\text{-}1Mn}$ = 993 K (720 °C), $T_{cast\_Al\text{-}10Si}$ = 903 K (630 °C), Q_{inner} = 700 L h^{-1}, and Q_{outer} = 1200 L h^{-1}).

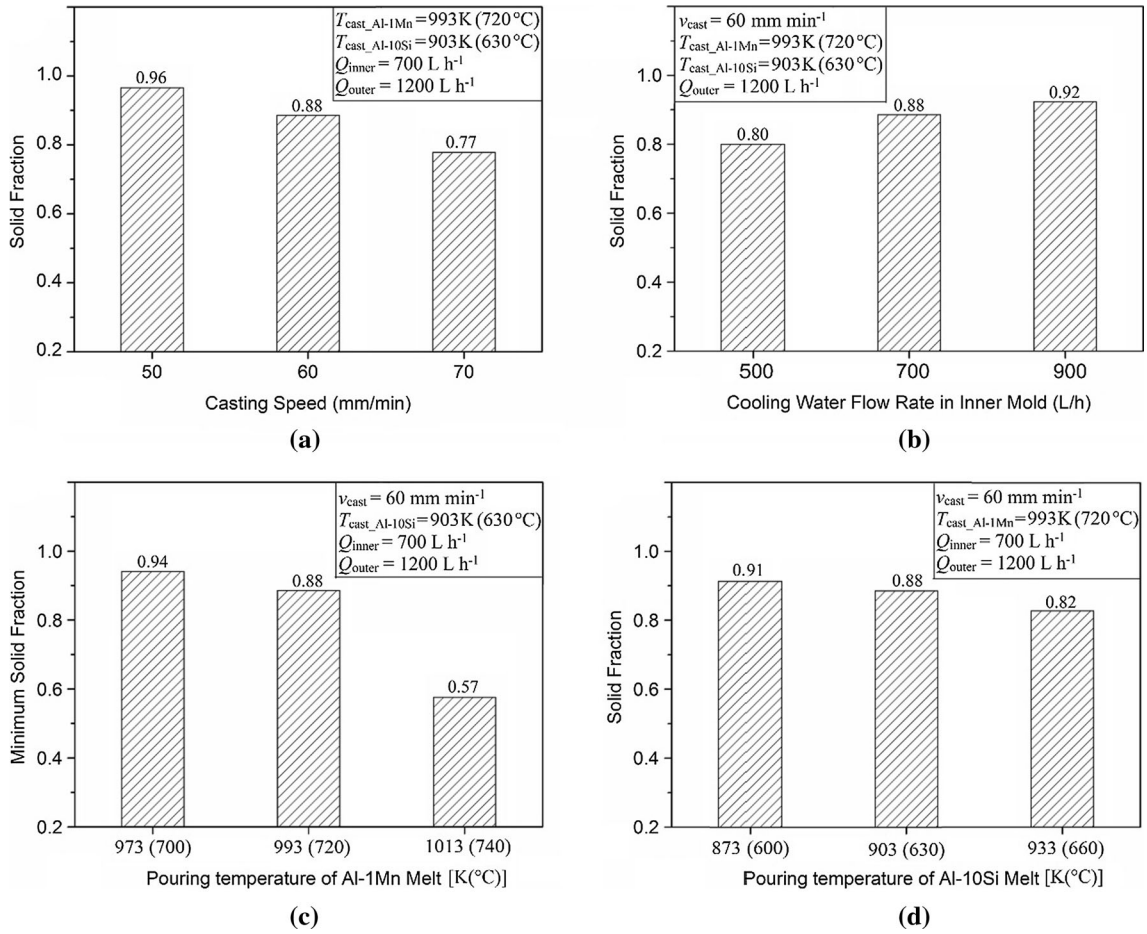

Fig. 6—Calculated variations of the minimum solid fraction on the Al-1Mn clad layer side of the interface with (*a*) casting speed, (*b*) cooling water rate in inner mold, (*c*) Al-1Mn casting temperature, and (*d*) Al-10Si casting temperature.

on both sides of the interface start to increase and finally reach unity at about 13 mm below the outer mold bottom due to the effects of the mold and secondary water cooling from clad layer of the ingot. In the interface zone when the Al-10Si melt first contacts with the Al-1Mn shell below the inner mold bottom, the clad layer shell of Al-1Mn is in mushy form and the core layer of Al-10Si is liquid as shown in Figure 5. This is good for the casting process since the liquid metal of core layer can wet the semisolid primary shell of clad layer at the interface, thereby creating a strong bond interface.

B. *Casting Practice Studies*

The results studying in Section IV–A are important to understand the physics of the casting process, and a better approach to understand the success and failure scenarios is to study the distribution of solid fraction at the interface of core and clad layers.

The minimum value of solid fraction at the interface can be used as a parameter to determine whether the semisolid primary shell of clad layer remains intact after contact with the liquid melt of core layer. It was used by Baserinia *et al.*[14] as a criterion for the survival of the semisolid shell. This minimum solid fraction value should be larger than an assumed threshold, and then, the semisolid primary shell will be strong enough to prevent a breakthrough of the Al-10Si liquid metal into the Al-1Mn sump at some location on the interface of core and clad layers and mixing of the two alloys. The coherency solid fraction of the two-phase material in the mushy zone is used to define the critical threshold for survival of the semisolid shell. Above the coherency solid fraction, the two-phase material in the mushy zone is coherent enough to begin to behave like a solid and is able to withstand normal stress and strain.[22] The coherency solid fraction for the Al-1Mn alloy is assumed to be 0.5.[23] If the minimum solid fraction is lower than the assumed "coherency solid fraction," then the difference in metallostatic pressures across the interface is predicted to cause a liquid breakthrough from the core layer sump into the clad layer and a failure of the casting process for preparing Al-1Mn/Al-10Si circular clad ingot.

Figure 6 shows the calculated variations of the minimum solid fraction on the Al-1Mn clad layer side of the interface with the casting speed, cooling water rate in inner mold, and casting temperature of Al-1Mn melt and Al-10Si melt, respectively. The results indicate

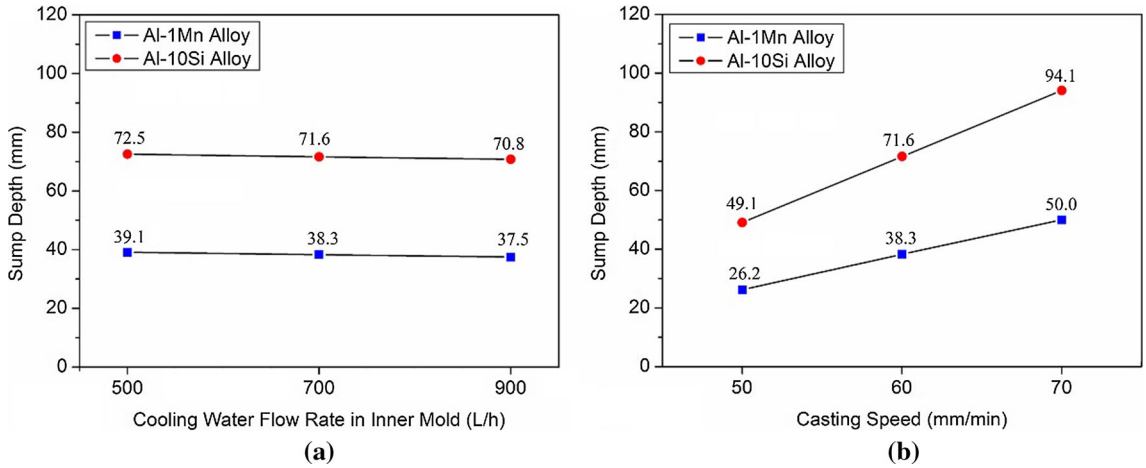

Fig. 7—Maximum sump depth with respect to the surface of Al-1Mn melt as a function of (*a*) cooling water flow rate in inner mold and (*b*) casting speed.

that the effect of casting speed and Al-1Mn casting temperature on the variations of the minimum solid fraction of Al-1Mn at the interface is stronger than that of cooling water flow rate in inner mold, while Al-10Si casting temperature is the weakest of the four casting parameters. The different degree effect of casting temperature of Al-1Mn and Al-10Si melts is because that the latent heat of fusion of Al-1Mn is smaller than that of Al-10Si. As seen, the minimum solid fraction of Al-1Mn at the interface correlates directly with the cooling water flow rate in inner mold and inversely with the casting speed, Al-1Mn and Al-10Si casting temperature. In other words, increasing the cooling water flow rate in inner mold and reducing the casting speed and casting temperatures lead to more favorable conditions to maintain the interface of the clad and core layers and prevent liquid metal breakthroughs from the Al-10Si to the Al-1Mn sump through the initial Al-1Mn primary shell. Figure 6 also shows that the minimum solid fraction of Al-1Mn at the interface ranges from 0.96 to 0.57 with different casting conditions. That is to say, a sufficiently strong primary shell at the interface is provided in terms of coherency of the semisolid shell under these casting conditions explored in the current study.

Figure 7 shows the predicted maximum sump depth of both the core and clad layers of the ingot below the surface of Al-1Mn melt. Here, the sump depth is defined as the distance between the surface of Al-1Mn melt and the coherency temperature line of two alloys. As can be seen, the sump depth increases with increasing casting speed, but is almost independent of the cooling water flow rate in inner mold. This is because the sump depth is primarily influenced by the secondary water cooling, whereas the inner mold cooling is typically very small compared to the secondary water cooling.

C. *Experimental Verification*

A circular clad ingot of Al-1Mn and Al-10Si alloys was successfully prepared by direct chill casting with the same experimental parameters as the typical case presented before. Metallographic observation, electron probe microanalysis (EPMA), tensile testing, and Vickers hardness testing were carried out in order to investigate the microstructure morphology and mechanical properties of the interface of the clad ingot.

The images of transverse section and microstructures of the interface of the clad ingot are shown in Figure 8. As seen in Figure 8(a), the Al-1Mn and Al-10Si alloys are distinctly separated into the clad layer and core layer because of the different surface color after etching (the Al-10Si shown in Figure 8(a) always appears slightly darker than the Al-1Mn because of their different chemical compositions), and the interface is clear with few casting defects. In addition, there is an acceptable bonding at the interface zone as shown in Figure 8(b). For the Al-10Si alloy of core layer, the microstructure contains the dendritic α-Al phase and a eutectic structure with fine acicular Si, while on the clad side, a few Al_6Mn particles are distributed in the Al matrix.

When the Al-10Si melt contacts with the Al-1Mn semisolid shell below the inner mold bottom, the solute diffusion occurs at the interface. The Si element diffuses from the Al-10Si side to the Al-1Mn side because the Al-10Si alloy side is relatively enriched with Si atoms. In the meantime, the Mn element diffuses in the opposite direction at the interface. Figure 9 shows the solute distribution of the Mn and Si elements in the diffusion zone of the clad ingot measured by EPMA. As seen, the content of the Si element is about 1.6 pct at the position of 20 μm away from the interface on the Al-10Si alloy side and decreases gradually to about 0.2 pct at the position of 20 μm away from the interface on the Al-1Mn alloy side. However, the diffusion distance of the Mn element is much shorter than that of the Si element. The main reason is that the concentration gradient of the Mn element in the diffusion zone is lower than that of the Si element, and the diffusion coefficient of the Si element in Al matrix is higher than that of Mn under the same condition.[24] The diffusion zone is

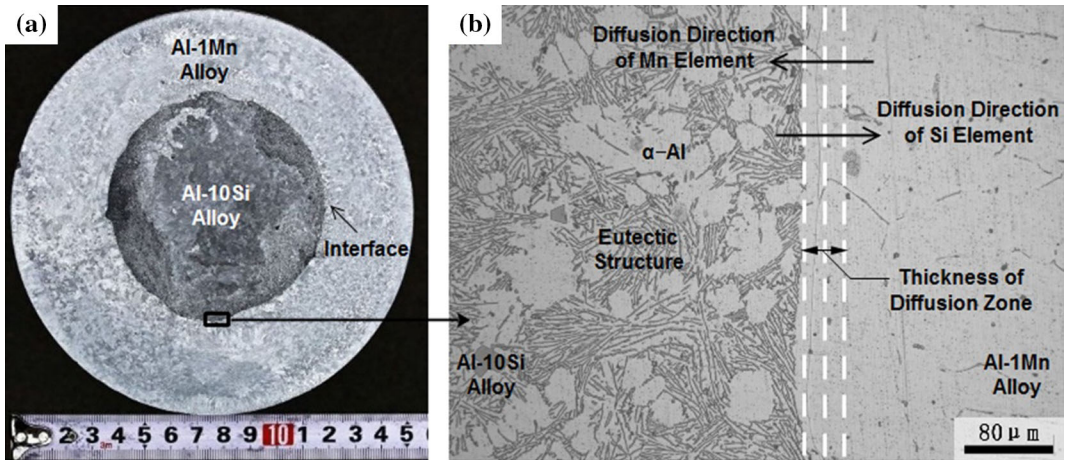

Fig. 8—The images of (*a*) transverse section of and (*b*) microstructures of the interface of the clad ingot.

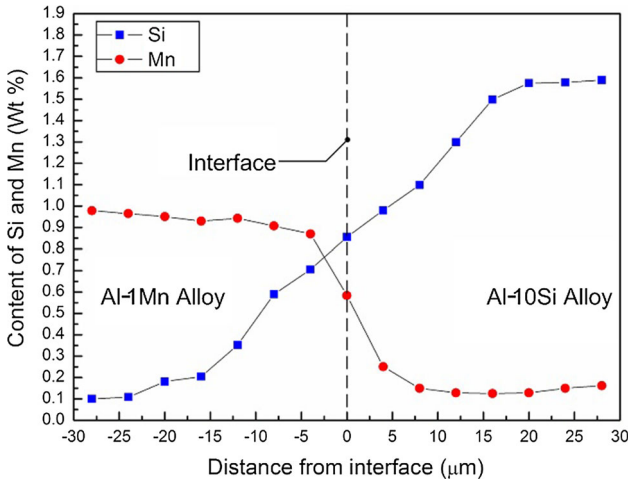

Fig. 9—The content of Mn and Si elements in the diffusion zone measured by EPMA.

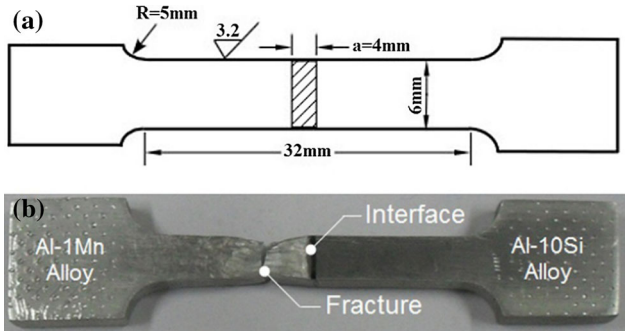

Fig. 10—(*a*) Shape and size of tensile sample and (*b*) the tensile fractured specimen.

formed by the interdiffusion of the Si and Mn elements into the matrix of counterparts. In the present experiment, the thickness of diffusion zone between Al-10Si and Al-1Mn alloys is defined as the distance that Si content decreases from average to minimum value across the interface. According to the results of EPMA in Figure 9, the diffusion zone is marked by white dash dot lines in Figure 8(b).

Tensile test was performed using a ZwickBZ2.5/TS1S test machine with a strain rate of 1 mm/min to examine the interface strength. The shape and size of tensile sample is shown in Figure 10(a) according to GB/T 16865-1997 standard. Figure 10(b) shows the fractured tensile sample with the interface zone marked and the tensile strength of the sample is 106.8 MPa. It can be seen that the fracture occurs in the Al-1Mn alloy side, while the interface remains well, which indicated that the strength of the interfacial region is higher than that of Al-1Mn alloy, and the tensile strength of the interface is more than 106.8 MPa. The interface strength is higher than in the Al-1Mn alloy due to the effect of solid solution strengthening, but it should be lower than that of Al-10Si alloy. This is because that plasticity should predominantly occur in the softer alloy and failure occurs when the ultimate tensile strength (UTS) of Al-1Mn is reached if a clean and high strength interface is formed between the two different alloys.

Figure 11 shows the Vickers microhardness measurement across the interface of the Al-1Mn alloy and Al-10Si alloy. The specimen surface was carefully polished before testing. The test was performed on the sample surface using a typical diamond indenter in the form of a pyramid with a square base and an angle of 136 deg between opposite faces. The load was 1.96 N which was applied for 15 seconds. As seen, the microhardness of Al-1Mn alloy is in the range of 35–40 HV, while it is in the range of 76–82 HV for the Al-10Si alloy. In addition, the microhardness of the interface zone is higher than that of the Al-1Mn alloy, but lower than that of the Al-10Si alloy. Both hardness and strength are important properties of materials, and they often obey the three times empirical relationship,[25] *i.e.*, $HV \approx 3\sigma_y$, where HV is the Vickers microhardness, and σ_y is the yield strength. Thus, it can be

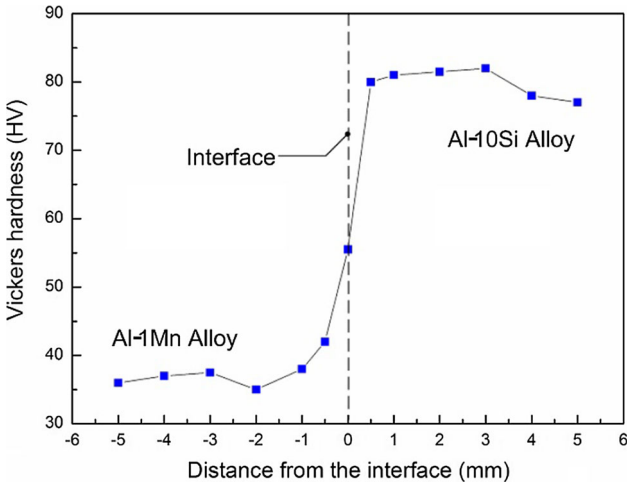

Fig. 11—Vickers hardness values across the interface region.

concluded that the interface yield strength is also higher than that of the Al-1Mn alloy.

V. CONCLUSIONS

In the current study, a comprehensive simulation model was developed to investigate the direct chill casting process based on Novelis Fusion™ Technology for preparing the Al-1Mn/Al-10Si circular clad ingot, and a parametric study and experimental research of the direct chill casting process was conducted to understand the potential success and failure casting conditions. The simulation results revealed the bonding mechanism of the Al-1Mn/Al-10Si interface in the direct chill casting process and identified the effect of certain parameters on casting performance. The results indicated that the effect of casting speed and Al-1Mn casting temperature on the variations of the minimum solid fraction of Al-1Mn at the interface is stronger than that of cooling water flow rate in inner mold, while Al-10Si casting temperature is the weakest of the four casting parameters. The minimum solid fraction of Al-1Mn at the interface correlates directly with the cooling water flow rate in inner mold and inversely with the casting speed, Al-1Mn and Al-10Si casting temperature. A sufficiently strong primary shell at the interface can be provided in terms of coherency of the semisolid shell under these casting conditions explored in the current study.

The corresponding experimental results verified that Al-1Mn/Al-10Si circular clad ingot with acceptable metallurgical bonding can be successfully prepared by direct chill casting process under the proper casting parameters. The main bonding pattern of bimetal materials is diffusion bonding because of diffusion of Si and Mn elements and the thickness of diffusion zone is about 40 μm. Both the tensile strength and the Vickers microhardness of the interfacial region are higher than that of Al-1Mn alloy.

ACKNOWLEDGMENTS

The authors gratefully acknowledge the supports of the National Natural Science Foundation of China (Nos. 51274054, U1332115, 51271042, 51375070, 51401044), the Keygrant Project of Chinese Ministry of Education (No. 313011), the Science and Technology Planning Project of Dalian (No. 2013A16GX110), the China Postdoctoral Science Foundation (2014M551075), and the Fundamental Research Funds for the Central Universities.

REFERENCES

1. W.S. Miller, L. Zhuang, J. Bottema, A. Wittebrood, P. De Smet, A. Haszler, and A. Vieregge: *Mater. Sci. Eng. A*, 2000, vol. 280, pp. 37–49.
2. B. Zhu, W. Liang, and X.R. Li: *Mater. Sci. Eng. A*, 2011, vol. 528, pp. 6584–88.
3. X.P. Zhang, T.H. Yang, S. Castagne, and J.T. Wang: *Mater. Sci. Eng. A*, 2011, vol. 528, pp. 1954–60.
4. M. Eizadjou, H.D. Manesh, and K. Janghorban: *Mater. Des.*, 2008, vol. 29, pp. 909–13.
5. D.J. Lloyd: *Scripta Mater.*, 2013, vol. 68, pp. 13–16.
6. A. Gupta, S.T. Lee, and R.B. Wagstaff: *Mater. Technol.*, 2007, vol. 22, pp. 71–75.
7. Y.J. Su, X.H. Liu, H.Y. Huang, C.J. Wu, X.F. Liu, and J.X. Xie: *Metall. Mater. Trans. B*, 2011, vol. 42, pp. 104–13.
8. N. Liu, J.C. Jie, Y.P. Lu, L. Wu, Y. Fu, and T.J. Li: *J. Mater. Process. Technol.*, 2014, vol. 214, pp. 60–66.
9. T. Wang, C. Liang, Z. Chen, Y. Zheng, H. Kang, and W. Wang: *J. Mater. Process. Technol.*, 2014, vol. 214, pp. 1806–11.
10. C. Nerl, M. Wimmer, H. Hoffmann, E. Kaschnitz, F. Langbein, and W. Volk: *J. Mater. Process. Technol.*, 2014, vol. 214, pp. 1445–55.
11. W. Shyy, Y. Pang, G.B. Hunter, D.Y. Wei, and M.H. Chen: *Int. J. Heat Mass Transf.*, 1992, vol. 35, pp. 1229–45.
12. J.K. Yoon: *Isij Int.*, 2008, vol. 48, pp. 879–84.
13. M.J. Feng, E.G. Wang, and J.C. He: *Acta Metall. Sini.*, 2011, vol. 47, pp. 1495–512.
14. A.R. Baserinia, E.J.F.R. Caron, M.A. Wells, D.C. Weckman, S. Barker, and M. Gallerneault: *Metall. Mater. Trans. B*, 2013, vol. 44B, pp. 1017–29.
15. E. Foroozmehr, S. Esmaeili, D.J. Lloyd, and M. Gallerneault: *Metall. Mater. Trans. A*, 2012, vol. 43A, pp. 1770–80.
16. E.J.F.R. Caron, R.E.O. Pelayo, A.R. Baserinia, M.A. Wells, D.C. Weckman, S. Barker, and M. Gallerneault: *Metall. Mater. Trans. B*, 2014, vol. 45B, pp. 975–87.
17. Y. Fu, J. Jie, L. Wu, J. Park, J. Sun, J. Kim, and T. Li: *Mater. Sci. Eng. A*, 2013, vol. 561, pp. 239–44.
18. C.Y. Wang, S. Ahuja, C. Beckermann, and H.C. Degroh: *Metall. Mater. Trans. B*, 1995, vol. 26B, pp. 111–19.
19. H. Zhang, H. Nagaumi, Y. Zuo, and J. Cui: *Mater. Sci. Eng. A*, 2007, vol. 448, pp. 189–203.
20. J. Sengupta, S.L. Cockcroft, D.M. Maijer, M.A. Wells, and A. Larouche: *Metall. Mater. Trans. B*, 2004, vol. 35B, pp. 523–40.
21. D.C. Weckman and P. Niessen: *Metall. Trans. B*, 1982, vol. 13B, pp. 593–602.
22. A. Stangeland, A. Mo, O. Nielsen, D. Eskin, and M. M'Hamdi: *Metall. Mater. Trans. A*, 2004, vol. 35A, pp. 2903–15.
23. M.G. Pokorny, C.A. Monroe, C. Beckermann, Z. Zhen, and N. Hort: *Metall. Mater. Trans. A*, 2010, vol. 41A, pp. 3196–207.
24. Y. Du, Y.A. Chang, B.Y. Huang, W.P. Gong, Z.P. Jin, H.H. Xu, Z.H. Yuan, Y. Liu, Y.H. He, and F.Y. Xie: *Mater. Sci. Eng. A*, 2003, vol. 363, pp. 140–51.
25. K.M. Youssef, R.O. Scattergood, K.L. Murty, and C.C. Koch: *Scripta Mater.*, 2006, vol. 54, pp. 251–56.